ELSEVIER

International Journal of Heat and Fluid Flow 19 (1998) 31–38

International Journal of HEAT AND FLUID FLOW

Examination of interfacial shape and onset of slugging of a stratified flow at a combining Y-junction

Wang Kee In [a], Sang Yong Lee [b,*]

[a] *Korea Atomic Energy Research Institute, 150 Dukjin-Dong, Yusong-Gu, Taejon 305-353, South Korea*
[b] *Department of Mechanical Engineering, Korea Advanced Institute of Science and Technology, 373-1 Kusong-Dong, Yusong-Gu, Taejon 305-701, South Korea*

Received 22 November 1996; accepted 23 June 1997

Abstract

The interface profile and the pressure distribution of a stratified flow and the critical conditions for slug formation at a combining Y-junction are examined experimentally. Air flows through the nearly horizontal channel, and water is introduced into the airstream through the bottom slit. The water-layer thickness and the pressure distribution along the upper wall of the main channel are measured. The critical air velocities for the slug formation are also measured for a range of water-inlet velocity conditions. The effects of the air–water-inlet velocities, the channel inclination angle, and the water-injection angle are studied in this experiment. Basically, the water layer shows a peak near the merging point and then approaches to an equilibrium level far downstream. At the larger water-injection angle, another water-layer peak is observed slightly downstream of the primary peak. The pressure drops sharply near the merging point because of the acceleration of the air flow and then gradually rises up to a certain level at the downstream where the pressure rise by the air flow deceleration and the pressure drop by the friction are balanced. The slugging occurs when the air velocity exceeds an interfacial instability condition. The critical air velocity decreases with the increase of the water-injection angle or the water-inlet velocity. An empirical criterion for slugging at a combining Y-junction is also proposed.

Keywords: Stratified flow; Slugging; Combining Y-junction; Gas–liquid interface

Notation

g	gravitational acceleration (m/s^2)
h	channel height (m)
K	constant
V	velocity (m/s)
x	horizontal coordinate
y	vertical coordinate

Greek

β	channel inclination angle (deg)
ϕ	ratio of the liquid (water) momentum to gas (air) momentum
θ	water-injection angle (deg)
ρ	density (kg/m^3)

Subscripts

f	liquid (water)
g	gas (air)
o	air–water inlet
p	water-layer peak
s	interface

* Corresponding author.

0142-727X/98/$19.00
PII: S0142-727X(97)10006-6

1. Introduction

Many of the two-phase pipe lines used in the process industries have relatively small length-to-diameter ratios, and the internal flow pattern largely depends on the geometrical inlet conditions as well as on the properties and the flow rates of gas and liquid. A typical way of mixing the gas and the liquid is to inject the liquid into the gas stream through a wall slot. In this case, a separated flow pattern (stratified flow or annular flow) is observed near the mixing point; then, depending on the flow condition, it develops into the dispersed or intermittent flow pattern as it flows downstream. The flow pattern transition is initiated when the relative velocity between gas and liquid layers exceeds an interfacial instability condition as can be seen in the Kelvin–Helmholtz-type instability analysis (Lamb, 1932); and to find out the instability criteria, the steady-state flow behavior should be understood prior to the instability analysis. A number of studies have reported on the stability of the straight stratified flow because the steady-state shape of its interface is known to be flat a priori (Taitel and Dukler, 1976; Lin and Hanratty, 1986; Crowley et al., 1992; Barnea and Taitel, 1993). However, with the bottom wall injection (Fig. 1), the steady interface becomes curved, and its exact profile should be obtained prior to the instability analysis. Hence, the experimental data on the steady-state interface

profile and the pressure drop, and on the condition of the slug formation at the combining Y-junction, would be very useful for future numerical calculations and instability analysis. In other words, either linear or nonlinear instability analysis can be performed by perturbing the measured steady-state interface profiles. The experimental data on the interface profiles can be used to confirm the validity of the numerical calculations. Once the numerical approaches are proved to be correct, an instability analysis can be performed by perturbing the steady-state solution at various conditions.

Several published results are available on the two-phase flow mixing and distribution at pipe junctions. Kubo and Ueda (1973) reported experimental data on the flow distribution into the branches for air–water mixtures in the horizontal piping systems with a confluent header. They examined the effects of the geometrical dimensions on the pressure loss and on the ratio of the flow rate through branch pipes. Lilly et al. (1975) reported the experimental results on steam/water mixing that may occur in loss of coolant accident (LOCA) of pressurized water reactors (PWR). Emergency core-cooling water is injected into the cold leg through a side branch with an angle. There it mixes with the steam returning from the steam generators and flows into the reactor vessel. Mixing and condensation are the primary phenomena observed at the point of injection. The performance of cooling is partially determined by the pressure drop at the mixing point; thus, the pressure drop data across the mixing point were obtained so that a steady-state cold-leg resistance model could be developed. The effects of the injection angle, steam velocity, system pressure, and the water-injection velocity were examined in this work. Kubie and Gardner (1978) investigated the air–water flow through symmetrical combining Y-junctions connected to containers. Their investigation is limited to the equal stratified flows in each inclined limb approaching the junction. They studied the change of the flow regime by controlling the water flow rate. Schmidt and Loth (1994) developed the semiempirical correlations to predict the two-phase pressure drop at a combining T-junction. They considered the cases of the upward annular and churn flows in a vertical pipe with its top end connected to a horizontal pipe with the slug or annular flow in it.

There are also a series of studies for small-scale gas–liquid mixing, such as the characterization of the Y-jet atomizer used in oil burners. Gas and liquid are supplied through each inlet port and mixed internally within the mixing port (tube). Mullinger and Chigier (1974) conducted an experimental work to examine the atomization performance change with the Y-jet atomizer geometry. As a part of their work, they measured the pressure drop inside the atomizer and proposed the relationships between the pressure drop and the flow rates of the atomizing fluid (air) and fuel. They also examined the blockage effect of the fuel and air; that is, increasing of the fuel-flow rate reduces the air-flow rate when the constant air supply pressure is maintained. However, the blockage effect of the atomizing air (on the fuel-flow rate) turned out to be insignificant except at the small fuel-flow rates. Hurley and Doyle (1985) obtained the correlations on the flow coefficients counting the blockage effect by measuring fuel/air mass flow rates and injection pressures. The ENEL-CRTN group, including Graziadio et al. (1987), De Michele et al. (1989, 1991), and Andreussi et al. (1992), also has performed the studies on the flow characteristics inside the two-phase port and obtained the relationship between the injection pressures and the flow rates of the gas and the liquid. These studies were based on the one-dimensional compressible flow approach. The presence of the liquid phase was accounted for with a modified frictional coefficient. However, their results are not able to predict the flow rates unless the mixing point pressure is known a priori. Hence, Lee et al. (1992) and In et al. (1993) developed a simplified one-dimensional mechanistic model to predict the pressure drop across the two-phase port, and the results were compared with the measurements. They assumed an annular-mist flow within the two-phase port, and the blockage effects were also considered. However, their model may be valid in limited operating ranges, because the experiments for comparison were performed only within narrow ranges.

Based on these works, in the present study, the behavior of a two-dimensional stratified flow at a combining Y-junction, as shown in Fig. 1, was examined experimentally. Air is supplied from the left-hand side to the main channel, and water is discharged through the bottom branch, which is connected to the main channel with an angle θ. The main channel is tilted down from horizon by an angle β. It is noted in Fig. 1 that point B is the air–water merging point, and point O is the corner point where the water flow separation may occur. The interface profile and the upper-wall pressure distribution of the curved stratified flow and the critical conditions for the slug formation were measured for various angles of the channel inclination and the water injection as well as for various air–water inlet velocities. An empirical slugging criterion at a combining Y-junction is also proposed in this paper.

2. Experiments

The schematic of the experimental setup used in this study is shown in Fig. 2. Air and water were used as the test fluids in this experiment. The air was supplied to the test section through an air-settling chamber. A screen and a honeycomb were installed within the air-settling chamber to improve the uniformity of the flow. Water at room temperature was injected into the test section through a water-settling chamber connected to the constant head tank. Similarly, a screen was placed within the water-settling chamber to make the flow uniform. The water-flow rate was measured with a calibrated flow meter (FLT-N, Flow Cell) at the inlet of the water-settling chamber. The air-flow rate was measured with a flow nozzle installed inside the air-settling chamber. The flow nozzle was manufactured according to the ASME standards on the fluid meters (Bean, 1971) and calibrated by measuring air velocities at the nozzle exit. The errors in the measurements of the water-flow rate and the air-flow rate are bounded by ±0.15 lpm (±0.01 m/s in water-inlet velocity) and ±6.0 lpm (±0.2 m/s in air-inlet velocity), respectively. These errors include the calibration error, the scale-reading error, etc.

The test section is made of acrylic for flow visualization. The main (and air) channel height ($h_{g,o}$) is 10 mm and the width of the water channel slit ($h_{f,o}$) is 5 mm. The depth of the channel is 50 mm, which is believed to be large enough for the two-dimensional assumption. The total length of the

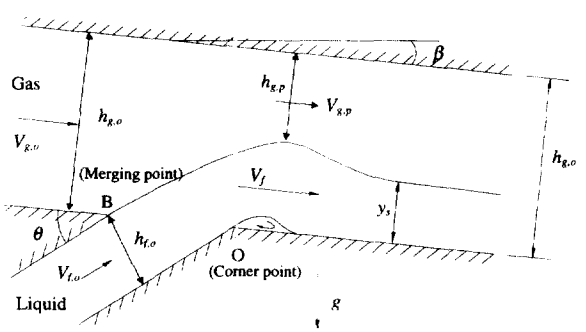

Fig. 1. Gas–liquid merging flow at a Y-shaped junction.

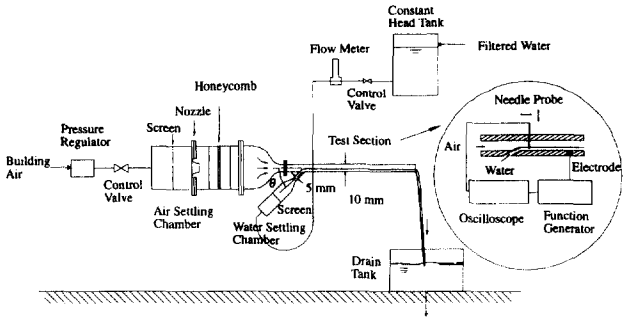

Fig. 2. Schematic of experimental setup.

test section between the air inlet and the exit is 400 mm. The pressure taps and the needle probe holes are placed at the upper plate.

A needle contact probe was used to measure the interface profile (mean water-layer thickness). The needle tip was sharpened to increase the local resolution and to minimize the measurement error originating from the surface tension effect. An electrode was installed at the lower plate. The needle contact probe was adjusted by using a screw attached to the micrometer head scaled with an interval of 0.01 mm. The measurement error of the water-layer thickness is estimated to be ±0.08 mm with the allowances for the surface tension effect as well as for the micrometer scale. Details of the measuring device for the interface profile is also shown in Fig. 2. The pressure distributions along the upper wall were measured using a pressure transducer within an accuracy of ±2.45 N/m^2.

Two cases of the water-injection angle θ were tested, i.e., 30° and 60°, and the effect of the channel inclination angle β was tested for 1.8°, 5.3°, and 8.5°, respectively. Basically, the experiments were performed under the atmospheric pressure condition. The water- and air-inlet velocities were changed within 0.19–0.51 and 2.72–8.33 m/s, respectively. The water-layer thickness was measured at nine locations along the centerline towards the downstream from the merging point. The distance between the measuring points was kept as close as possible near the merging point and was increased as it went downstream. The differential pressures, referenced to the air-inlet pressure, were also measured at seven locations. The onset of slugging was judged by flow visualization.

3. Slugging criteria

Instability criteria for straight stratified flow have been developed by many investigators. Two types of Kelvin–Helmholtz analyses have been used: the inviscid Kelvin–Helmholtz (IKH) theory in which the shear stresses are neglected and the viscous Kelvin–Helmholtz (VKH) analysis, which uses the full two-fluid model with the shear stresses.

The classical inviscid Kelvin–Helmholtz theory (Lamb, 1932; Milne-Thomson, 1963) provides an instability criterion for slugging as follows.

$$V_g \geq K\left[\frac{(\rho_f-\rho_g)gh_g}{\rho_g}\right]^{1/2} \tag{1}$$

with the value of K being the unity that overpredicts the gas velocity for slugging by a factor of two. Wallis and Dobson (1973) proposed 0.5 for K for the slugging criterion from the experimental data. Taitel and Dukler (1976) proposed a theoretical model for predicting flow regime transitions in horizontal and near-horizontal gas–liquid flow. They considered the pressure difference over the wavy surface due to the Bernoulli effect. They postulated the slugging would occur when the pressure difference exceeds the gravity force acting on the wave. They proposed the same criterion for the slugging in two-dimensional horizontal channels and in circular pipes as Eq. (1) with the coefficient K, which depends on the size of the wave; for an infinitesimal disturbance, K approaches to 1.0, and for a finite disturbance, K is less than unity. Similarly, Kordyban (1977) obtained the same criterion from the force-balance concept over the wave, but with the inverse of constant K estimated to be 1.35 from the experimental data. Mishima and Ishii (1980) theoretically obtained the value of K in Eq. (1) for horizontal flows. The value of K was determined by introducing the concept of the "most dangerous wave," and, finally, they proposed 0.487 for K for the slug formation criterion.

VKH analysis has been performed by Wallis (1969), Lin and Hanratty (1986), Wu et al. (1987), Andritsos and Hanratty (1987), Barnea (1991) and Crowley et al. (1992), and Barnea and Taitel (1993, 1994). They derived the equation for neutral stability starting from the full two-fluid model and taking account of the shear stresses. Many of the VKH stability criteria were compared with the Taitel and Dukler (1976) criterion, because it is the most widely used correlation form to predict the slug formation. Barnea (1991) and Barnea and Taitel (1993) noticed that neither VKH nor IKH theories by themselves provide an adequate criterion between the stratified flow and the slug (or annular) flow. Hence, a combined model incorporating both the IKH and the VKH analyses was proposed.

The neutral stability equation based on the VKH analysis is too complex to apply and even gives unacceptable criteria under a certain condition. Thus, the Taitel and Dukler (1976) criterion (with appropriate modifications) is most widely used for its simplicity in application to the straight stratified flow whose interface shape is known to be flat at the fully developed condition. However, the Taitel–Dukler criterion is not directly applicable to the combining Y-junction shown in Fig. 1, because the stratified flow at the junction is in a developing stage with a curved interface. In addition to the Bernoulli effect, the entrance effects (liquid injection angle, channel inclination, flow rates) should be considered somehow in the slugging criterion at the combining Y-junction. Therefore, in the present work, the slugging condition for the flow shown in Fig. 1 was deduced based on the Taitel and Dukler criterion with minor modification of the model constant K. In other words, the slugging criterion at a combining Y-junction is proposed to be

$$V_{g,p} \geq C_Y\left[\frac{(\rho_f-\rho_g)gh_{g,p}}{\rho_g}\right]^{1/2}, \tag{2}$$

where $V_{g,p}$ and $h_{g,p}$ denote the local average velocity of gas (air) and the height of the gas layer above the liquid (water) hump, respectively, as shown in Fig. 1. C_Y is the model constant to account for the entrance effects. Since $V_{g,p}$ is not known a priori, it is replaced with the gas velocity at the inlet boundary ($V_{g,o}$), but with further modification of the model constant C_Y to develop a practically useful slugging criterion as

$$V_{g,o} \geq C'_Y\left[\frac{(\rho_f-\rho_g)gh_{g,p}}{\rho_g}\right]^{1/2}, \tag{3}$$

where

$$C'_Y = C'_Y(\rho_f, \rho_g, V_{f,o}, V_{g,o}, \theta, \beta). \tag{4}$$

It is also noted that the relative height of the gas layer downstream of the merging point depends on the gas and liquid properties and flow rates as well as on the ratio between the channel heights of gas and liquid at the inlet. Hence, the height of the gas layer above the liquid hump $h_{g,p}$ can be expressed as

$$\frac{h_{g,p}}{h_{g,o}} = \frac{h_{g,o}}{h_{g,o} + h_{f,o}} C(\rho_f, \rho_g, V_{g,o}, V_{f,o}, \theta, \beta). \quad (5)$$

By inserting Eq. (5) into Eq. (3), the proposed criterion can be rewritten as

$$V_{g,o} \geq C_M \left[\frac{(\rho_f - \rho_g) g h'_g}{\rho_g} \right]^{1/2}, \quad (6)$$

where

$$h'_g \equiv \frac{h_{g,o}}{h_{g,o} + h_{f,o}} h_{g,o} \quad (7)$$

and

$$C_M = C'_Y C^{1/2}. \quad (8)$$

Here, from Eqs. (4) and (5), C_M should be a function of gas and liquid densities, flow rates, and the inlet geometry. However, the onset of slugging at a combining Y-junction is expected to depend largely on the inclination angle and the liquid–gas momentum ratio (rather than on those individual parameters), and the model constant C_M may be expressed as

$$C_M = C_1(\beta) C_2(\phi \sin\theta). \quad (9)$$

Here, ϕ indicates the water-to-air momentum ratio defined as

$$\phi \equiv \frac{\rho_f V_{f,o}^2}{\rho_g V_{g,o}^2}, \quad (10)$$

which is multiplied by $\sin\theta$ in Eq. (9) to account for the lateral momentum effect on the flow instability. Coefficients C_1 and C_2 are determined from the experimental results on the onset of slugging at the combining Y-junction.

4. Results and discussion

Fig. 3 shows the measured water-layer thickness and the upper-wall pressure distribution (referenced to the wall pressure at the air inlet) for the water-injection angle of 30°, the channel inclination of 5.3°, and the constant water-inlet velocity of 0.26 m/s. The air-inlet velocity varies from 2.72 to 4.69 m/s. As shown in Fig. 3(a), the water-layer thickness decreases as the air-inlet velocity increases. Irrespective of the air velocity, the water layer is thinning, and its thickness approaches almost to a single value as it flows downstream. It should be noted from Fig. 3(b) that the pressure drops significantly near the maximum thickness of the water layer because of the acceleration of the air flow. The lowest pressure is observed at about two times the air channel height (i.e., $x/h_{g,o} \approx 2$) downstream from the merging point; after that the wall static pressure is recovered because of the air flow deceleration and approaches to a certain value asymptotically. Also, the pressure drop becomes larger as the air-inlet velocity increases.

Fig. 4 shows the effect of the water-inlet velocity with the air-inlet velocity fixed to 3.59 m/s for the water-injection angle of 30° and the channel inclination of 5.3°. The water-inlet velocity was changed from 0.19 to 0.32 m/s. The water layer in Fig. 4(a) appears to be thicker, with its peak shifted to the downstream as the water-inlet velocity increases. This was also confirmed from the photograph shown in Fig. 5. Again, the upper-wall pressure in Fig. 4(b), referenced to the air-inlet pressure, shows the lowest value near the maximum water-layer thickness because of the acceleration of the air flow. As the water-inlet velocity increases, the air is more accelerated because of the narrower air passage, and the pressure drop becomes larger. Similar to the cases shown in Fig. 3(b), the upper-wall pressure reaches a minimum at the value of $x/h_{g,o}$ being about two and then starts to increase up to a certain

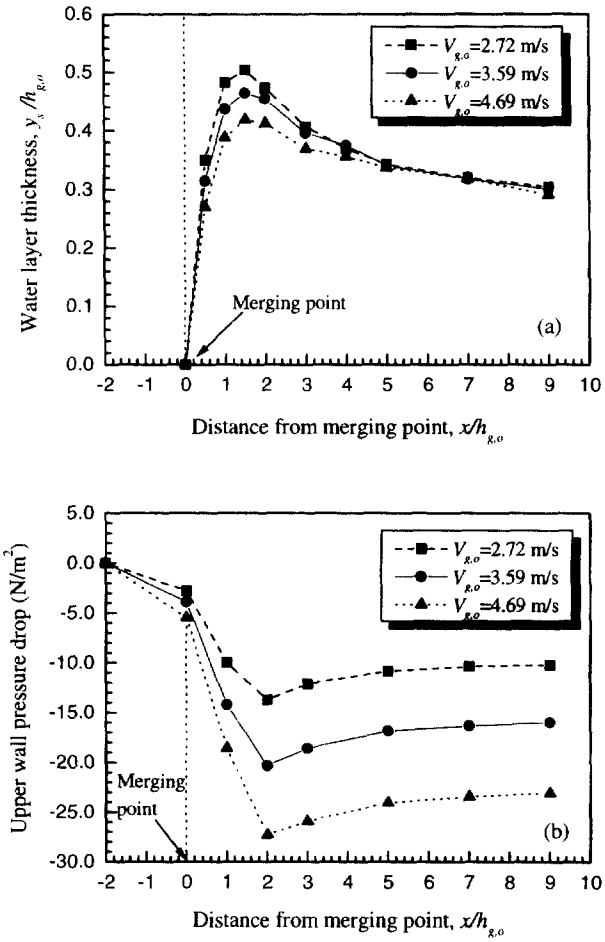

Fig. 3. Effect of air velocity for $\theta = 30°$, $\beta = 5.3°$, and $V_{f,o} = 0.26$ m/s: (a) interface profile; (b) upper-wall pressure distribution.

value where the pressure recovery by the air-flow deceleration and the pressure drop by the wall friction balance.

The effect of the channel inclination on the water-layer thickness and the upper-wall pressure distribution is shown in Fig. 6. The water layer with the larger inclination in Fig. 6(a) appears to be thinner because of the larger gravitational acceleration of the water flow. The height of the hump significantly decreases with the larger channel inclination; because of the thinner water layer, the pressure drop at the larger inclination angle becomes smaller for the same inlet velocity conditions as shown in Fig. 6(b).

Fig. 7 compares the interface profiles and upper-wall pressure distributions for different water-injection angles and air-inlet velocities when the channel inclination and the water-inlet velocity are fixed to 5.3° and 0.19 m/s, respectively. The water-layer peak near the merging point in Fig. 7(a) significantly increases for the larger water-injection angle. This is caused by the large discharge momentum in the lateral direction. However, it is interesting to note that the water-layer thicknesses at the far downstream are not much different between each other. This is because the effect of the geometry difference decreases at the downstream; furthermore, the effect of the air velocity on the water-layer thickness seems to be minor at the downstream, because the air density is much smaller than the water density. Also, it should be noted that, for the water-injection angle of 60°, the secondary peak is observed at approximately four times the air channel height ($x/h_{g,o} \approx 4$) downstream from the merging point. This secondary peak is

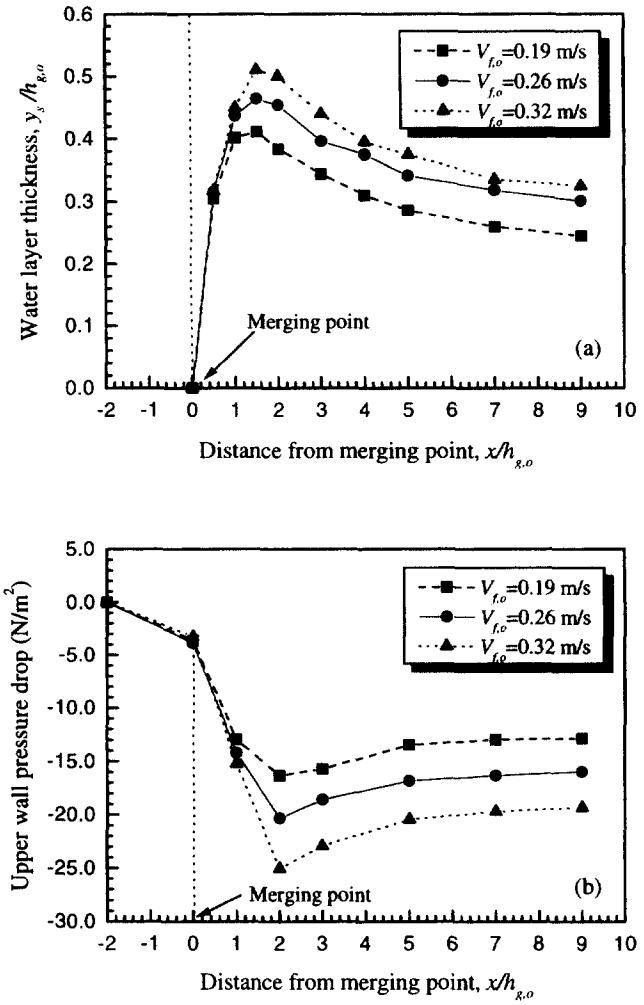

Fig. 4. Effect of water velocity for $\theta = 30^\circ$, $\beta = 5.3^\circ$, and $V_{g,o} = 3.59$ m/s: (a) interface profile; (b) upper-wall pressure distribution.

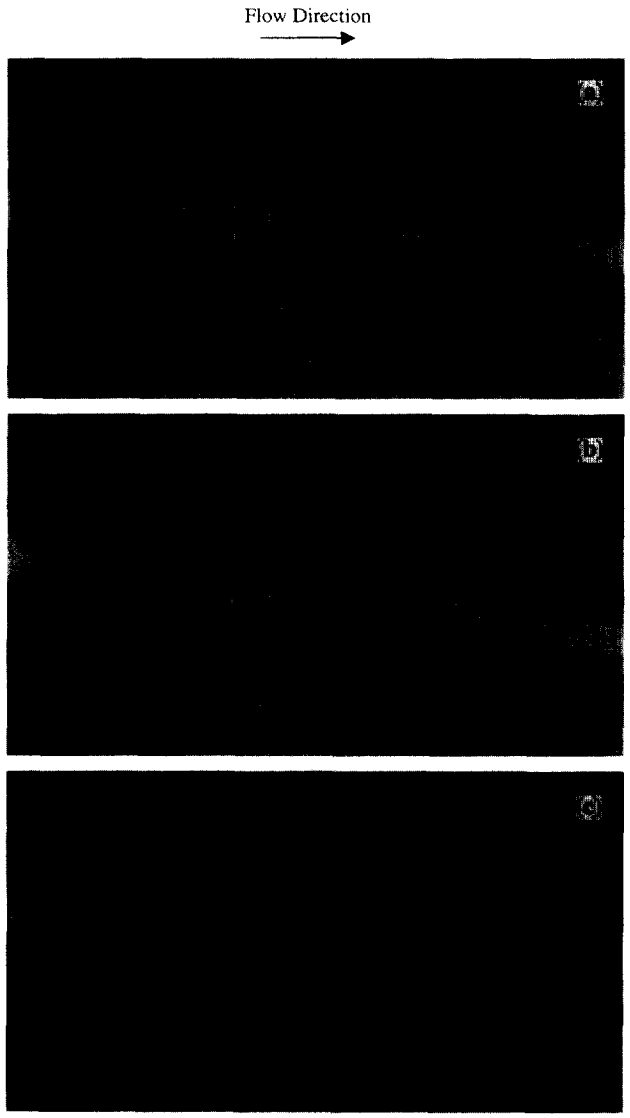

Fig. 5. Flow visualization of interface profiles for $\theta = 30^\circ$, $\beta = 5.3^\circ$, and $V_{g,o} = 3.59$ m/s: (a) $V_{f,o} = 0.19$ m/s; (b) $V_{f,o} = 0.26$ m/s; (c) $V_{f,o} = 0.32$ m/s.

considered to be a hydraulic jump (Chaudhry, 1993) formed when the flow changes from supercritical to subcritical flow. The larger water-injection angle would induce the larger flow separation at the corner point (point O in Fig. 1). The water flowing over the larger separation zone and then over the slightly inclined channel is similar to that flowing over a slope changing from steep to mild. Generally, a hydraulic jump occurs when the slope of the channel bottom changes from steep to mild. Fig. 7(b) compares the measured pressure distributions along the upper wall; generally the pressure sharply drops just after the merging point because of the air-flow acceleration, then recovers gradually by the air-flow deceleration. The pressure drop with the larger water-injection angle is bigger than that with the smaller injection angle because of the higher peak of water layer. However, it is noted that the upper-wall pressures with the same water-injection angles are getting close to each other in the pressure recovery region once the air- and water-inlet velocities are the same.

Fig. 8 shows the effects of the water-injection angle and the water-inlet velocity with the channel inclination and the air-inlet velocity fixed to 5.3° and 2.72 m/s, respectively. Similar to the case shown in Fig. 7, the double water-layer peaks are observed with the larger water-injection angle in Fig. 8(a). The primary peak occurs just after the merging point and the secondary peak at approximately four times the air-channel height ($x/h_{g,o} \approx 4$) downstream of the merging point. However, the water layers with the same inlet velocities of air and water tend to merge to each equilibrium level at the downstream of the secondary peak. Because of the higher primary peaks, the pressure drops with the larger injection angle and the higher velocity of water are remarkably bigger near the merging point as shown in Fig. 8(b). However, again, the effect of the geometry difference (injection angle) decreases in the pressure recovery region, and the pressures with the same inlet velocities of air and water are getting close to each other. Here, we can confirm that the entrance effect becomes minor at the downstream location.

Fig. 9 shows the critical air velocity for slug formation for different channel inclinations and water-injection angles for each water-inlet velocity. The slug flow was observed to occur at the downstream of the primary water-layer peak (hump). The small amplitude waves developed at the right downstream of the primary water-layer peak on increasing air velocity and then grew to a large amplitude wave. The development of the small amplitude waves seems to be expedited by the higher primary hump. The large amplitude wave grows downstream until it touches the upper wall when the

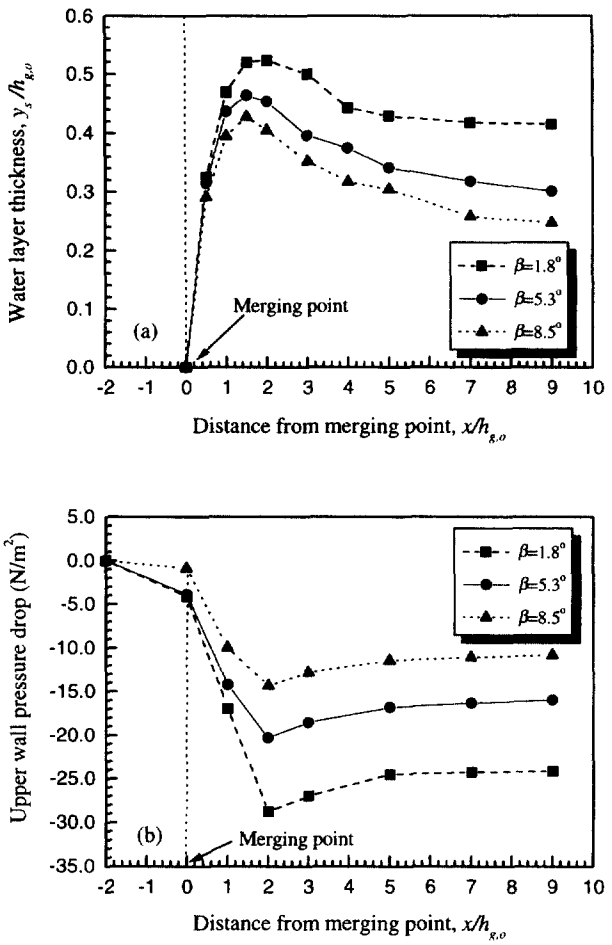

Fig. 6. Effect of channel inclination for $\theta = 30^\circ$, $V_{f,o} = 0.26$ m/s, and $V_{g,o} = 3.59$ m/s: (a) interface profile; (b) upper-wall pressure distribution.

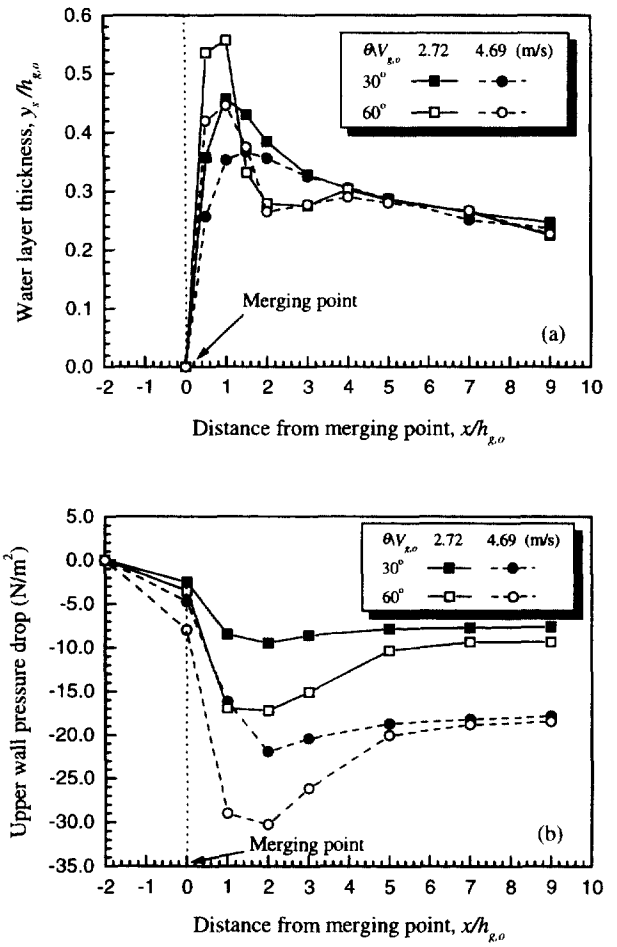

Fig. 7. Effects of water-injection angle and air velocity with $\beta = 5.3^\circ$ and $V_{f,o} = 0.19$ m/s: (a) interface profile; (b) upper-wall pressure distribution.

air velocity is increased further. The wave growth is enhanced if the secondary peak exists (for the larger water injection angle). The slugging was observed to occur periodically in accordance with generation and growth of the large amplitude wave. The critical air velocity decreases (that is, the slugging occurs easily) as the water-inlet velocity increases and/or the channel inclination angle decreases. This is because the larger water-inlet velocity and/or the smaller channel inclination angle result in the thicker water layer, which is more apt to form waves. The slug flow also occurs at lower air velocity with the larger water-injection angle because of the formation of the secondary peak.

Fig. 10 compares the thickness of the primary water-layer peak at the slug inception. For a constant water-injection angle θ, the critical peak thickness increases as the channel inclination angle β decreases. This is caused by the smaller gravity effect with the small channel inclination. For a fixed channel inclination angle, the critical peak thickness for larger water-injection angle seems to be higher because of the larger lateral momentum of water. It is also noted from Figs. 9 and 10 that the critical air velocity decreases as the primary peak of the water layer increases. This indicates that the primary peak of the water layer near the merging point has a destabilizing effect on the stratified-to-slug flow transition.

The coefficients C_1 and C_2 of the slugging criterion in Eq. (9) were tentatively determined by data fitting from the experimental results as

$$C_1(\beta) = 1.0 + 2.8 \sin \beta, \tag{11}$$

$$C_2(\phi \sin \theta) = 0.31 + 0.27e^{2.12\phi \sin \theta} + 0.32e^{-0.15\phi \sin \theta}. \tag{12}$$

The coefficient C_1 was determined from the experimental data for three different channel inclination angles. Then, the coefficient C_2 was determined from Eqs. (6) and (9), and C_1. The coefficient C_2 was well correlated to the ratio of the lateral momentum of water to the axial momentum of air ($\phi \sin \theta$) as shown in Fig. 11, and is represented by Eq. (12) satisfactorily. Therefore, once the water-inlet velocity $V_{f,o}$ is given, the coefficients C_1 and C_2 can be determined from Eqs. (11) and (12) along with Eq. (6). The critical air velocities obtained from Eqs. (6), (11) and (12) are plotted in Fig. 9, which seems to be in reasonable agreement with the measured ones. Therefore, it was confirmed that the flow pattern transition at the air–water combining junction is influenced by the ratio of the lateral momentum of water to the axial momentum of air, and depends on the geometrical inlet conditions as well as on the gas–liquid properties and flow rates.

5. Conclusions

The interface profile and the pressure distribution of a stratified flow and the critical conditions for slug formation at a combining Y-junction were examined experimentally.

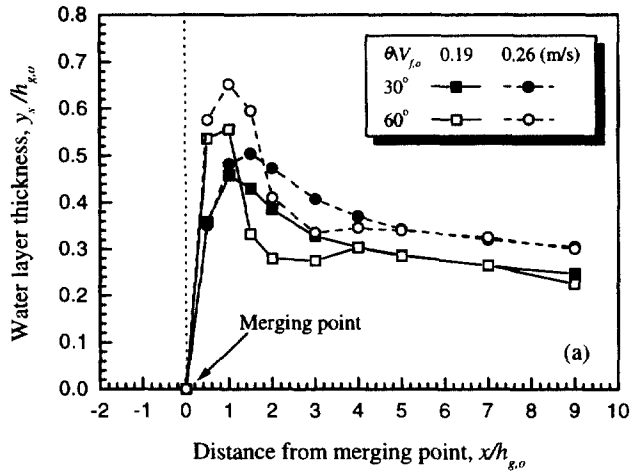

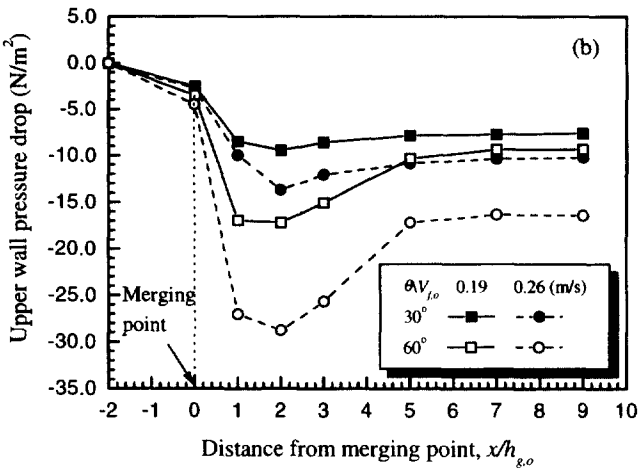

Fig. 8. Effects of injection angle and velocity of water with $\beta = 5.3°$ and $V_{g,o} = 2.72$ m/s: (a) interface profile; (b) upper-wall pressure distribution.

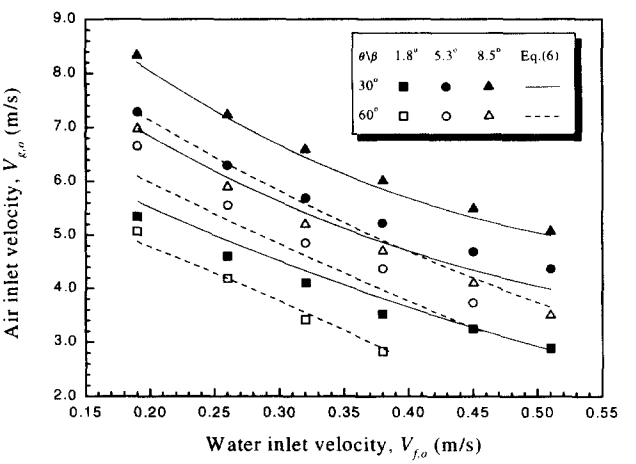

Fig. 9. Critical air velocity for slug formation.

Air flowed through the nearly horizontal channel, and water was introduced into the air stream through the bottom slit. The water-layer thickness and the pressure distribution along the upper wall of the main channel were measured. The critical

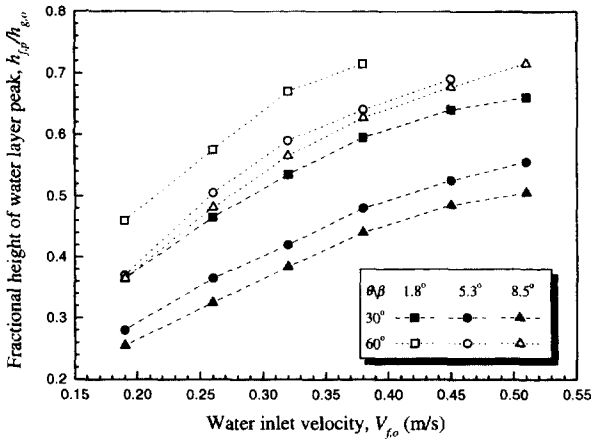

Fig. 10. Thickness of primary water-layer peak at the inception of slug flow.

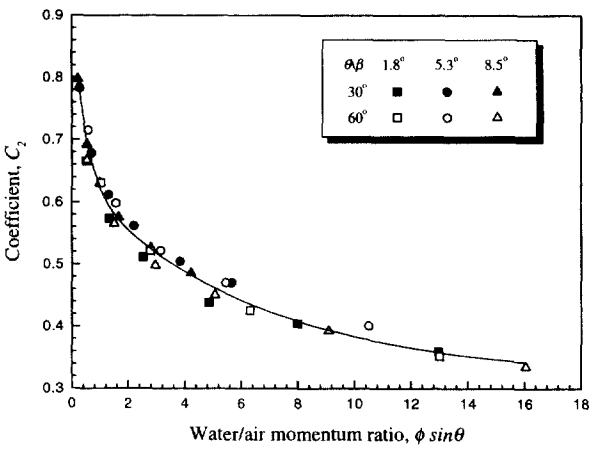

Fig. 11. Coefficient C_2 for the modified slugging criterion.

air velocities for the slug formation were also measured. The effects of the air–water inlet velocities, the channel inclination angle, and the water-injection angle were studied in this experiment. The water-layer peak was observed near the merging point; this peak decreased and shifted downstream as the air velocity or the channel inclination angle was increased. However, the interface profile showed a tendency to merge into an equilibrium shape far downstream for a fixed water-inlet velocity and channel inclination. For larger water-injection angle, the secondary water-layer peak was observed slightly downstream of the primary peak. The upper-wall pressure dropped sharply just after the merging point because of the air-flow acceleration (caused by the water-layer peak). Then the pressure recovered to an equilibrium value at the downstream where the pressure rise because of the air-flow deceleration and the pressure drop by friction balanced. As the air velocity was increased, the small amplitude waves were developed at the right downstream of the primary water-layer peak and then grew up to a large amplitude wave. Slugging occurred repeatedly in accordance with generation and growth of the large amplitude wave. The critical air velocity decreased as the water-injection angle or the water-inlet velocity was increased. An empirical slugging criterion was proposed to express the inception of the slug flow at a gas–liquid combining Y-junction.

Acknowledgements

The authors express their appreciation to the Korea Advanced Institute of Science and Technology (KAIST) and the Ministry of Science and Technology (MOST) of Korea for their financial support.

References

Andreussi, P., Tognotti, L., De Michele, G., Graziadio, M., 1992. Design and characterization of twin-fluid Y-jet atomizers. Atomization Sprays 2, 45–59.

Andritsos, N., Hanratty, T.J., 1987. Interfacial instabilities for horizontal gas–liquid flows in pipelines. Int. J. Multiphase Flow 13, 583–603.

Barnea, D., 1991. On the effect of viscosity on stability of stratified gas–liquid flow – Application to flow pattern transition at various pipe inclinations. Chem. Eng. Sci. 46, 2123–2131.

Barnea, D., Taitel, Y., 1993. Kelvin–Helmholtz stability criteria for stratified flow: Viscous versus non-viscous (inviscid) approaches. Int. J. Multiphase Flow 19, 639–649.

Barnea, D., Taitel, Y., 1994. Nonlinear interfacial instability of separated flow. Chem. Eng. Sci. 49, 2341–2349.

Bean, H.S., 1971. Fluid Meters: Their Theory and Application, 6th ed. ASME, United Engineering Center, New York.

Chaudhry, M.H., 1993. Open-Channel Flow. Prentice Hall, Englewood Cliffs, NJ.

Crowley, C.J., Wallis, G.B., Barry, J.J., 1992. Validation of a one-dimensional wave model for the stratified-to-slug flow regime transition, with consequences for wave growth and slug frequency. Int. J. Multiphase Flow 18, 249–271.

De Michele, G., Graziadio, M., Novelli, G., Andreussi, P., Giacomelli, A., 1989. Scaling problems of H.F.O. Y-jet atomizers. Proceedings of the Fourth Members Conference, Int. Flame Res. Found., Noordwijkernout, The Netherlands.

De Michele, G., Graziadio, M., Morelli, F., Novelli, G., 1991. Characterization of the spray structure of a large-scale H.F.O. atomizer. Proceedings of ICLASS-91, Gaithersburg, MD, pp. 779–786.

Graziadio, M., Andreussi, P., Tognotti, L., Zanelli, S., 1987. Atomization of coal–water fuels by a pneumatic internal mixing nozzle. Part I – Two-phase flow inside the nozzle. Atomisation Spray Technol. 3, 187–208.

Hurley, J.F., Doyle, B.W., 1985. Design of two-phase atomisers for use in combustion furnaces. Proceedings of ICLASS-85, 1A/3/1-1A/3/13.

In, W.K., Lee, S.Y., Song, S.H., 1993. Modeling of nozzle flow inside a Y-jet twin-fluid atomizer. Trans. KSME 17, 1841–1850.

Kordyban, E., 1977. Some characteristics of high waves in closed channels approaching Kelvin–Helmholtz instability. J. Fluids Eng. 99, 339–346.

Kubie, J., Gardner, G.C., 1978. Two-phase gas–liquid flow through Y-junctions. Chem. Eng. Sci. 33, 319–329.

Kubo, T., Ueda, T., 1973. On the characteristics of confluent flow of gas–liquid mixtures in headers. Bull. JSME 16, 1376–1384.

Lamb, S.H., 1932. Hydrodynamics, 6th ed. Dover, New York.

Lee, S.Y., Park, B.S., In, W.K., 1992. Study of flow characteristics inside a Y-jet twin-fluid atomizer. Proceedings of the Second JSME–KSME Thermal Engineering Conference, Kitakyushu, Japan.

Lilly, G.P., Stephens, A.G., Hochreiter, L.E., 1974. Mixing of emergency core cooling water with stream: 1/14-Scale testing phase. EPRI Guide 294-2, CA 94304.

Lin, P.Y., Hanratty, T.J., 1986. Prediction of the initiation of slugs with linear stability theory. Int. J. Multiphase Flow 20, 79–98.

Milne-Thomson, L.M., 1963. Theoretical Hydrodynamics. MacMillan, New York.

Mishima, K., Ishii, M., 1980. Theoretical prediction of onset of horizontal slug flow. J. Fluids Eng. 102, 441–445.

Mullinger, P.J., Chigier, N.A., 1974. The design and performance of internal multijet twin fluid atomizers. J. Inst. Fuel 47, 251–261.

Schmidt, H., Loth, R., 1994. Predictive methods for two-phase flow pressure loss in tee junctions with combining conduits. Int. J. Multiphase Flow 20, 703–720.

Taitel, Y., Dukler, A.E., 1976. A model for predicting flow regime transitions in horizontal and near horizontal gas–liquid flow. AIChE J. 22, 47–55.

Wallis, G.B., Dobson, J.E., 1973. The onset of slugging in horizontal stratified air–water flow. Int. J. Multiphase Flow 1, 173–193.

Wallis, G.B., 1969. One-Dimensional Two-Phase Flow. McGraw-Hill, New York.

Wu, H.L., Pots, B.F., Hollenberg, J.F., Meerhoff, R., 1987. Flow pattern transitions in two-phase gas/condensate flow at high pressure in an 8-inch horizontal pipe. Proceedings of the Third International Conference on Multi-phase Flow, The Hague, The Netherlands, pp. 13–21.